© 2014. Published by The Company of Biologists Ltd | The Journal of Experimental Biology (2014) 217, 1-5 doi:10.1242/jeb.097402

RESEARCH ARTICLE

The role of the olfactory recess in olfactory airflow

Thomas P. Eiting[1,*], Timothy D. Smith[2], J. Blair Perot[3] and Elizabeth R. Dumont[1,4]

ABSTRACT

The olfactory recess – a blind pocket at the back of the nasal airway – is thought to play an important role in mammalian olfaction by sequestering air outside of the main airstream, thus giving odorants time to re-circulate. Several studies have shown that species with large olfactory recesses tend to have a well-developed sense of smell. However, no study has investigated how the size of the olfactory recess relates to air circulation near the olfactory epithelium. Here we used a computer model of the nasal cavity from a bat (*Carollia perspicillata*) to test the hypothesis that a larger olfactory recess improves olfactory airflow. We predicted that during inhalation, models with an enlarged olfactory recess would have slower rates of flow through the olfactory region (i.e. the olfactory recess plus airspace around the olfactory epithelium), while during exhalation these models would have little to no flow through the olfactory recess. To test these predictions, we experimentally modified the size of the olfactory recess while holding the rest of the morphology constant. During inhalation, we found that an enlarged olfactory recess resulted in lower rates of flow in the olfactory region. Upon exhalation, air flowed through the olfactory recess at a lower rate in the model with an enlarged olfactory recess. Taken together, these results indicate that an enlarged olfactory recess improves olfactory airflow during both inhalation and exhalation. These findings add to our growing understanding of how the morphology of the nasal cavity may relate to function in this understudied region of the skull.

KEY WORDS: Olfaction, Modeling, Olfactory recess, Mammals

INTRODUCTION

In mammals thought to have a keen sense of smell (macrosmatic mammals), much of the olfactory epithelium lines a cul-de-sac at the back of the nose called the olfactory (Moore, 1981; Smith and Rossie, 2008; Smith et al., in press) or ethmoturbinal recess (Maier, 1993). The olfactory recess has only one opening, which allows it to sequester the air that is breathed in during inhalation and prevent it from washing out during exhalation. In this way, odorant-laden air that enters the olfactory recess has more time to circulate in the olfactory region and make contact with odor receptors (Yang et al., 2007). Having a well-developed olfactory recess thus likely improves olfactory performance in macrosmatic mammals (Craven et al., 2010; Yang et al., 2007). The development and extent of the olfactory recess varies considerably across mammals, from completely absent in, for example, hominoids and cetaceans (Moore, 1981; Smith et al., in press), to very large and well developed in groups such as canids (Craven et al., 2007). In this paper, we examine the effects of the extent of the olfactory recess on the patterns and rates of olfactory airflow.

The olfactory recess forms as the caudodorsal extension of the nasal fossa and is separated from the ventral nasopharyngeal ducts by a fully formed transverse lamina. The transverse lamina develops when the lateral walls of the vomer fuse to the medial projection of the lateral nasal wall (Smith and Rossie, 2008) (Fig. 1). The transverse lamina and other structures that bound the olfactory recess derive, in great part, from the mesenchymal condensation known as the pars posterior (De Beer, 1937; Moore, 1981; Smith and Rossie, 2008), so the variation in the development of these structures likely contributes to variation in the size of the olfactory recess across mammals.

One clade of mammals that exhibits substantial variation in the extent of the olfactory recess is the New World leaf-nosed bats (Family Phyllostomidae). One way to quantify this difference is to calculate the percentage of olfactory epithelium contained within the olfactory recess. This parameter relates to the size of the olfactory recess because, in all species examined, virtually all of the olfactory recess is lined with olfactory epithelium. We have found that some species have less than 10% of their total olfactory epithelium located within the olfactory recess, while other species have a third or more of their olfactory epithelium located within the olfactory recess (T.P.E., unpublished). In this study, we examine the hypothesis that an enlarged olfactory recess improves olfactory airflow in phyllostomid bats. To examine this hypothesis, we generated a steady-state model of airflow through the nasal passage of the short-tailed fruit bat, *Carollia perspicillata* (Linnaeus), and compared it with airflow predicted from models in which we artificially reduced and enlarged the olfactory recess. This species is common throughout much of the New World tropics, and it is often used in experimental and behavioral work, including previous work on olfactory sensitivity and discrimination (Laska, 1990a; Laska, 1990b; Thies et al., 1998). *Carollia perspicillata* lies near the base of the radiation of frugivores within the phyllostomids, and it is morphologically intermediate between the long-nosed nectar-feeding bats and the short-nosed canopy frugivores (Dumont et al., 2012; Freeman, 1988; Freeman, 2000). These two features make this species a well-suited model to study olfactory airflow.

If an enlarged olfactory recess improves olfactory airflow, then at a given volumetric flow rate, we expect nasal passages with an enlarged olfactory recess to have lower rates of flow (i.e. volume of flow per unit time) through the olfactory region during inhalation, which increases residence time of odorant molecules in the airspace above the olfactory mucosa (Craven et al., 2010; Yang et al., 2007). Long residence time is thought to improve absorption efficiency, meaning that proportionally more odorant molecules are absorbed in the mucus (Lawson et al., 2012). Second, we predict that models with an enlarged olfactory recess will have lower rates of airflow and less total airflow through the olfactory recess during exhalation. Lower rates of flow in the olfactory recess during exhalation would mean that air within the olfactory recess will 'wash out' relatively

[1]Graduate Program in Organismic and Evolutionary Biology, University of Massachusetts Amherst, Amherst, MA 01003, USA. [2]School of Physical Therapy, Slippery Rock University, Slippery Rock, PA 16057, USA. [3]Department of Mechanical and Industrial Engineering, University of Massachusetts Amherst, Amherst, MA 01003, USA. [4]Department of Biology, University of Massachusetts Amherst, Amherst, MA 01003, USA.

*Author for correspondence (tpeiting@bio.umass.edu)

Received 23 September 2013; Accepted 17 February 2014

The Journal of Experimental Biology (2014) doi:10.1242/jeb.097402

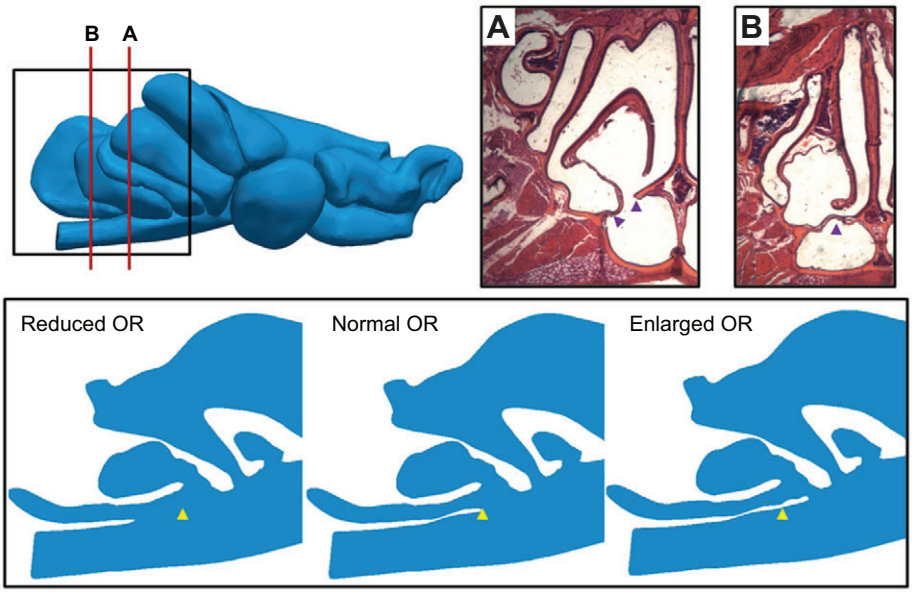

Fig. 1. Lateral view of right nasal airway, with anterior towards the right. The two red lines correspond to the anterior-posterior location of the two labeled histology slides, which show the formation of the transverse lamina. In A, the transverse lamina (TL) has not formed, but the lateral extensions of the vomer/nasal septum have nearly reached the medial projection of the lateral wall of the airway (purple arrowheads). In B, the TL has formed from the merger of the lateral extension of the vomer/septum and the medial extension of the lateral wall (purple arrowhead). The black box surrounding the back ~1/3 of the airway in the top left corresponds to the portion of the model shown in the bottom panel. This bottom panel illustrates the same parasagittal section roughly midway through the airway (i.e. parallel to the plane of the page), with each section coming from one of our three computational models. Reduced OR, model with transverse lamina reduced such that only ~7.5% of the total olfactory epithelium lies within the olfactory recess (OR); normal OR, unmodified model of *Carollia perspicillata*, in which 21.5% of the olfactory epithelium lies within the OR; enlarged OR, model with a lengthened transverse lamina such that ~33% of the total olfactory epithelium lies within the OR. In all three slices, the yellow arrowhead points to the anterior extreme of the TL as found in the normal OR model.

slowly. Furthermore, less air moving through the olfactory recess during exhalation would suggest that proportionately less air is washed out of the olfactory recess with each breath cycle, giving odorants more time in the olfactory recess to be absorbed.

RESULTS

Flow patterns in our computational models for the case of inhaled air support the prediction that a reduced olfactory recess produces higher flow velocities in the olfactory region (Fig. 3). We found that airflow in the reduced olfactory recess subvolume was 28% faster on average than in the normal olfactory recess subvolume (11.56×10^{-3} versus 9.06×10^{-3} m s^{-1}). Similarly, airflow in the normal olfactory recess subvolume was an average of 17% faster than in the enlarged olfactory recess subvolume (9.06×10^{-3} versus 7.74×10^{-3} m s^{-1}). When comparing the reduced olfactory recess versus the enlarged olfactory recess subvolumes, the average flow in the reduced olfactory recess subvolume was nearly 50% faster than in the enlarged olfactory recess subvolume (11.56×10^{-3} versus 7.74×10^{-3} m s^{-1}). Higher flow velocities translate to higher rates of flow in these models. This can be seen in the slice shown in Fig. 3, which corresponds approximately to the first anterior-posterior slice in which the olfactory recess appears. Flow rate into the olfactory recess at the level of the slice shown in Fig. 3 was highest in the reduced olfactory recess model (6.49×10^{-4} l min^{-1}), moderate in the normal olfactory recess model (3.46×10^{-4} l min^{-1}), and lowest in the enlarged olfactory recess model (1.27×10^{-4} l min^{-1}).

Qualitative comparisons between the three models during exhalation show that more streamlines pass through the same coronal anterior-posterior slice in models with a reduced olfactory recess (Fig. 4). For our quantitative comparisons, we calculated average flow rates for air leaving the olfactory recess at the same anterior-posterior slice as in the streamline comparison. Average rates of flow out of the olfactory recess at this slice were highest in the model with the reduced olfactory recess (5.1×10^{-4} l min^{-1}), moderate in the model with the normal olfactory recess (2.25×10^{-4} l min^{-1}), and lowest in the model with the enlarged olfactory recess (6.6×10^{-5} l min^{-1}).

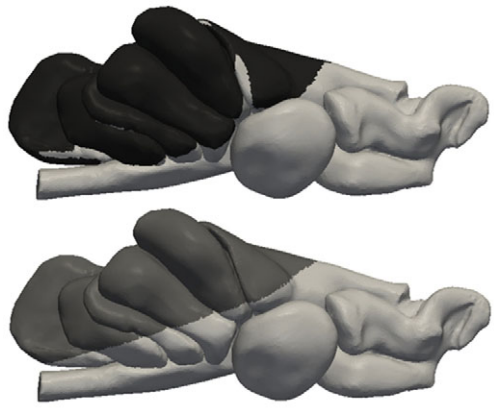

Fig. 2. Comparison of the location of the olfactory epithelium (black in the top image) with the location of our subvolume used to calculate flow rates during inhalation (gray in the bottom image). Note the approximate overlap between the colored portions of each image. The subvolume in the bottom image was selected based not only on its approximation to the location of the olfactory epithelium, but also on ease and reproducibility of its selection.

DISCUSSION

Computational studies of airflow in mammals have established that the olfactory recess is a region of the nasal fossa that is well-suited

The Journal of Experimental Biology (2014) doi:10.1242/jeb.097402

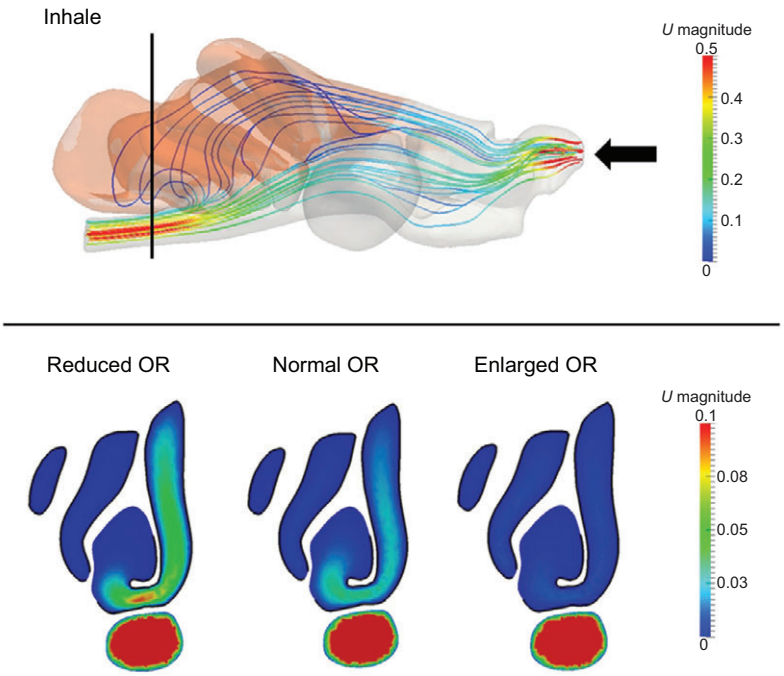

Fig. 3. Flow rates during inhalation in *Carollia perspicillata*. The top panel shows a lateral view of the whole airway, with anterior towards the right. Flow is in the direction of the black arrow. The location of the olfactory epithelium is shown in orange. The vertical bar shows the location of the first anterior-posterior slice with a complete transverse lamina (i.e. a fully sequestered olfactory recess). This slice forms the basis for comparisons in the bottom panel. See Fig. 1 legend for model descriptions. *U* magnitude refers to the velocity magnitude in m s^{-1}. Note the higher flow rates in the reduced OR model, and the lower flow rates in the elongated OR model.

for olfaction (Craven et al., 2010; Yang et al., 2007; Zhao et al., 2006). A small fraction of air inhaled during breathing and/or sniffing bypasses the respiratory region of the nose by a dorsal conduit, and then slows down upon entering the convoluted olfactory region, which ends in the blind olfactory recess. This study is the first to modify the size of the olfactory recess in order to understand whether and how much of an impact it has on altering olfactory airflow. We have demonstrated that the size of the olfactory recess contributes significantly to the flow patterns and rates of flow through the olfactory region. These results have implications for an improved understanding of the role that morphology plays in nasal airway function. The simulations of inspiratory airflow produced a steady increase in flow rates (which reduces molecule residence times) through the olfactory region in models with progressively reduced olfactory recesses. Comparing the extreme cases, the flow rate through the olfactory region of these models was ~50% higher in the reduced olfactory recess model compared with the enlarged olfactory recess model. These results indirectly support the hypothesis that the size of the olfactory recess, which is determined by the extent of the transverse lamina, can play a significant role in improving residence time of odorants within the olfactory region. This increase in residence time is predicted to produce a greater fractional uptake of odorants from the total mass flow of odorants at the inlet. To further examine odorant absorption in *C. perspicillata*, we would need to perform simulations of nasal odorant deposition.

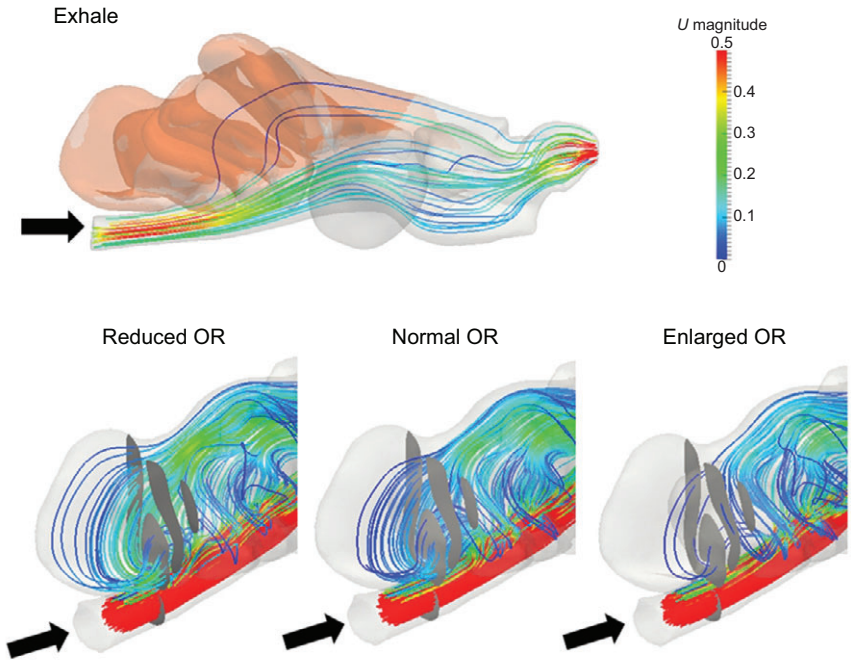

Fig. 4. Flow patterns during exhalation in *Carollia perspicillata*. The top panel shows a lateral view of the whole airway, with anterior towards the right. Flow is in the direction of the black arrows. The bottom panel shows an oblique latero-posterior view; the grey area is a slice from the same anterior-posterior location across all three models at the beginning of the olfactory recess. See Fig. 1 legend for model descriptions. *U* magnitude refers to the velocity magnitude in m s^{-1}. Note that progressively fewer streamlines pass through the slice in models with a longer transverse lamina (i.e. enlarged olfactory recess). Also note how the streamlines that do pass through the olfactory recess are on average slower (more blue in color) in the models with larger olfactory recesses.

On exhalation, we saw that as the olfactory recess was enlarged (by elongating the transverse lamina), rates of flow declined. Air that is already in the olfactory recess would thus be pushed out slowly, potentially allowing more time for odorant deposition in this region. We also saw progressively fewer streamlines passing through the olfactory recess as it was enlarged. This predicts that less air is washed out of the olfactory recess as the transverse lamina increases in length. This, in turn, would suggest that odorant molecules, on average, have more time to be absorbed into the mucus overlying the olfactory epithelium, and thereby have a greater chance of coming into contact with olfactory receptors. A fully transient simulation would be needed to investigate the interplay between inhalation and exhalation, and the extent to which inhaled airstreams become entrained in the olfactory recess before being washed out by exhaled air currents.

If increasing the size of the olfactory recess improves odorant residence times, what prevents an animal from elongating the transverse lamina so much that the olfactory becomes nearly completely closed off? The explanation is likely multifaceted, encompassing both developmental and functional constraints. The olfactory recess develops in concert with the rest of the nasal fossa, the midface and the braincase. As a result, the size, position and shape of the olfactory recess are probably limited by the developing forebrain, eyes and dentition (Moore, 1981; Smith and Rossie, 2008; Smith et al., in press). In addition, the respiratory functions of the nasal fossa (e.g. water retention, filtering) depend on having a large surface area over which air currents must pass. All else being equal, an enlarged olfactory recess would decrease the area and volume available for respiration, especially in short-faced species (Van Valkenburgh et al., 2004; Smith et al., in press).

How can our results be understood in light of studies that have shown that increasing flow rate (including sniffing) actually improves olfactory performance, rather than reducing it (e.g. Tucker, 1963; Oka et al., 2009)? These studies reason, quite correctly, that high flow rates imply that more odorant molecules can pass over the olfactory mucosa within a given period of time, thereby enhancing the olfactory system's ability to sense the odors.

The issue is resolved by focusing on the definition of olfactory performance. If the goal is to smell a 'packet' of odor that is highly localized, such as the odor trail of a plant or another bat, then processing more air (with higher flow rates) does not help the performance of the system. High flow rates in this case just add more air that does not contain the signal of interest. However, a low flow rate allows whatever odor exists in that packet of air to have the maximum time to trigger the sensory system. Put another way, the issue is one of temporal or spatial resolution (if the bat or the air is moving). If the odorant is distributed widely so that high flow rates can be assured of continually delivering air with more of the odorant, then a high flow rate might be an effective means of sampling. However, many odor signals are not distributed evenly or continuously in the environment. A classic study by Mozell et al. (Mozell et al., 1984) found that for a given volume of inhaled air, increasing the flow rate has a negative influence on the olfactory response. This is because if the goal is to process a localized 'whiff' of odorant, then it is more effective to slow the packet of air down as much as possible and give the system as much time as possible to be activated.

Sniffing likely improves olfactory processing by combining benefits of both high flow rates initially and low or no flow later. The early sniff involves a large flow rate to rapidly access a large volume of air and as may odorant molecules as possible. The later sniff involves a quiescent period where the net flow rate is almost zero, which lets the system have as much time as possible to trigger the olfactory sensory neurons from the packet of air that has just been obtained. Though we simulated airflow at the predicted high end of inspiratory flow rates, we have yet to simulate sniffing in an unsteady manner, which is required to more accurately capture patterns and rates of flow during a sniff. We hope to carry out such simulations in the future, which will aid in our understanding of how the dynamics of sniffing impact olfactory airflow.

Our study shows that variations in the size of the olfactory recess likely have significant functional consequences in groups that exhibit extensive variation in olfactory recess size, such as bats and primates (Cave, 1973; Moore, 1981; Smith et al., 2011; Smith et al., 2012; Smith et al., in press). This work also adds to the growing body of computational modeling studies that investigate the role of morphology in airway function. This computational approach allowed us to assess the potential role of just one morphological variable in affecting nasal airflow. We found that relatively minor modifications to the extent of the olfactory recess can have rather dramatic effects on flow patterns and rates through the olfactory recess. How might other aspects of the morphology relate to differences in flow? How do these morphological differences affect other aspects of nasal airway function, such as respiration or echolocation? Developing methods to adequately address these and other similar questions should contribute fundamentally to our understanding of how this complex region of the skull works.

MATERIALS AND METHODS

We constructed an anatomically accurate 3D finite volume model of the right nasal airway of an adult fluid-preserved *Carollia perspicillata* (AMNH #261433) from a microCT scan (X-Tek HMX ST 225; 72 kV, 148 µA, voxel size: 2.425×10^{-2} mm). We used Mimics v. 15.01 (Materialise, Leuven, Belgium) and Geomagic Studio v. 12.0 (3D Systems, Rock Hill, SC, USA) to create a solid model of the airway from the raw stack of CT image slices. Our relatively low-energy CT scan allowed us to see the air–mucosa boundary throughout much of the scan. In areas where the mucosa could not reliably be distinguished from the surrounding airspace, we consulted slices from a histological preparation of this same specimen of *C. perspicillata* (see details below), which allowed us to see the olfactory mucosa throughout the specimen. We matched the histology slices with the CT slices from the same locations, allowing us to modify the 3D model as needed. We artificially elongated the nasopharyngeal meatus (posterior opening of the nasal cavity) of our model by ~1.1 mm, to ensure that the flow during exhalation was fully developed at the back of the airway. The model of the air space included approximately 625,000 four-noded tetrahedral elements. We carried out a sensitivity study with twice the number of tetrahedra and found no appreciable differences in our results, so we used the 625,000 model in this study. To make the histological preparation of our specimen, the head was removed and decalcified in a solution of formic acid and sodium citrate. The specimen was then embedded in paraffin and sectioned on a rotary microtome at nominally 10 µm thickness in the coronal plane.

We mounted every fifth section and stained most slides with hematoxylin and eosin. Some intervening sections were also mounted and stained with Gomori trichrome or thionine. The histological preparations allowed us to examine the location and extent of the olfactory epithelium. We acquired photomicrographs of the sections and used ImageJ software to outline the olfactory epithelium in every third section. We then calculated the amount of olfactory epithelium section-by-section and the cumulative rostro-caudal percentage of olfactory epithelium for the entire specimen. This process allowed us to calculate that 21.5% of all of the olfactory epithelium was located in the olfactory recess (beginning with the first coronal section with a complete transverse lamina) for this specimen.

We also used histological slides to map the olfactory epithelium onto the 3D models. This was done by creating a surface model (STL file) of the olfactory mucosa in Geomagic Studio based on photomicrographs of the histology slides. Anatomical landmarks in the slides were matched to

the same landmarks in the original model of the airway in Geomagic. Once completed, this new STL file of the olfactory mucosa was imported directly into the flow visualization software (Paraview v. 3.98.1, Kitware, Inc., Clifton Park, NY, USA).

To examine the effects of enlarging or shrinking the olfactory recess, we altered the length of the transverse lamina in the *C. perspicillata* model. By lengthening the transverse lamina, we were able to create a model that had a proportionately larger olfactory recess. Similarly, shortening the transverse lamina produced a proportionately smaller olfactory recess. We altered the length of the transverse lamina in the model so that it enclosed an olfactory recess that contained the extremes of variation seen among phyllostomids (i.e. ~7.5% and ~34% olfactory epithelium within the olfactory recess; Fig. 1). These alterations were performed by artificially shortening and lengthening the transverse lamina using the modeling software (Geomagic Studio and Mimics).

We assessed steadiness in flow by calculating the Womersley number, which is a value used to distinguish steady from unsteady flow in fluids (Loudon and Tordesillas, 1998). For our study, the Womersley number was less than 1 (0.38), meaning that we could assume steady flow. The Reynolds number for the nasal airway of *C. perspicillata* is on the order of ~20, so we also assumed laminar flow. We applied the same volumetric flow rate to the models during both inhalation and exhalation. The flow rate was determined to be 2.255×10^{-2} l min^{-1}, based on the allometric equation suggested by Craven et al. (Craven et al., 2010):

$$Q_{\text{peak}} = 1.43M^{1.04}, \quad (1)$$

where Q_{peak} is peak inspiratory flow rate (l min^{-1}) and M is body mass (g). For our models, we used a value of 18.5 g for M, which is the average body mass of male *C. perspicillata* (Cloutier and Thomas, 1992). To apply this flow rate at the inlet (i.e. at the nostril during inhalation or at the choana during exhalation), we converted volumetric flow rate into fluid velocity assuming a constant inflow velocity, using the following equation:

$$U = Q/A, \quad (2)$$

where U is the fluid velocity (m s^{-1}), and A is the area of the inlet normal to the direction of flow (units???). In the presented simulations, the velocity is 0.78 m s^{-1} during inhalation and 0.29 m s^{-1} during exhalation. We applied a zero velocity gradient, constant pressure boundary at the outlet (i.e. at the choana during inhalation or at the nostril during exhalation).

Our quantitative analyses were performed as follows. For our inhalation case, we defined an identical subvolume in all three models that roughly matched the location of the olfactory epithelium (Fig. 2). For every cell in this subvolume, we extracted values for velocity magnitude, which were then used to calculate average airflow velocity. These average values were compared across the three models. We also calculated volumetric flow rate. First we selected an identical transverse slice in all three models that corresponded to the anterior-most beginning of the transverse lamina in the reduced olfactory recess model. Then we then integrated flow velocity across the area of this slice to calculate volumetric flow rate. We calculated volumetric flow rate for the exhalation case in the same manner and across the same slice. We also performed qualitative comparisons of flow passing through the olfactory recess by comparing flow patterns using streamlines (i.e. lines of flow tangential to the direction of flow). The streamlines were generated by 'seeding' a sphere (radius 0.35 mm) of 500 points near the choana.

Acknowledgements
We thank Nancy Simmons and Eileen Westwig, American Museum of Natural History, for access to the bat specimen used in this study. Nancy Forger and Geert DeVries generously provided access to the lab equipment used in the histological sampling. Mike Martell, Chris Zusi and Yang Song provided assistance with the CFD techniques. We thank members of the Dumont Lab, the Behavior and Morphology group at the University of Massachusetts, and two anonymous reviewers for comments on earlier versions of this manuscript.

Competing interests
The authors declare no competing financial interests.

Author contributions
T.P.E., T.D.S., J.B.P. and E.R.D. designed the study; T.P.E. performed the experiments and analyzed the data; and T.P.E., T.D.S., J.B.P. and E.R.D. prepared the manuscript.

Funding
This work was supported by a National Science Foundation (NSF) Doctoral Dissertation Improvement Grant (DEB-1110641 to T.P.E.) and the NSF Division of Biological Infrastructure (DBI-0743460 to E.R.D.). This work was performed in part at the Center for Nanoscale Systems (CNS) of Harvard University, a member of the National Nanotechnology Infrastructure Network (NNIN), which is supported by the National Science Foundation (ECS-0335765).

References

Cave, A. (1973). The primate nasal fossa. *Biol. J. Linn. Soc. Lond.* **5**, 377-387.
Craven, B. A., Neuberger, T., Paterson, E. G., Webb, A. G., Josephson, E. M., Morrison, E. E. and Settles, G. S. (2007). Reconstruction and morphometric analysis of the nasal airway of the dog (*Canis familiaris*) and implications regarding olfactory airflow. *Anat. Rec.* **290**, 1325-1340.
Craven, B. A., Paterson, E. G. and Settles, G. S. (2010). The fluid dynamics of canine olfaction: unique nasal airflow patterns as an explanation of macrosmia. *J. Roy. Soc. Interface* **7**, 933-943.
De Beer, G. (1937). *The Development of the Vertebrate Skull*. Oxford: Clarendon Press.
Dumont, E. R., Dávalos, L. M., Goldberg, A., Santana, S. E., Rex, K. and Voigt, C. C. (2012). Morphological innovation, diversification and invasion of a new adaptive zone. *Proc. R. Soc. B* **279**, 1797-1805.
Freeman, P. W. (1988). Frugivorous and animalivorous bats (Microchiroptera): dental and cranial adaptations. *Biol. J. Linn. Soc. Lond.* **33**, 249-272.
Freeman, P. W. (2000). Macroevolution in microchiroptera: recoupling morphology and ecology with phylogeny. *Evol. Ecol. Res.* **2**, 317-335.
Laska, M. (1990a). Olfactory discrimination ability in short-tailed fruit bat,carollia perspicillata (Chiroptera: Phyllostomatidae). *J. Chem. Ecol.* **16**, 3291-3299.
Laska, M. (1990b). Olfactory sensitivity to food odor components in the short-tailed fruit bat, *Carollia perspicillata* (Phyllostomatidae, Chiroptera). *J. Comp. Physiol. A* **166**, 395-399.
Lawson, M., Craven, B., Paterson, E. and Settles, G. (2012). A computational study of odorant transport and deposition in the canine nasal cavity: implications for olfaction. *Chem. Senses* **37**, 553-566.
Loudon, C. and Tordesillas, A. (1998). The use of the dimensionless Womersley number to characterize the unsteady nature of internal flow. *J. Theor. Biol.* **191**, 63-78.
Maier, W. (1993). Cranial morphology of the therian common ancestor, as suggested by the adaptations of neonate marsupials. In *Mammal Phylogeny: Mesozoic Differentiation Multituberculates, Monotremes, Early Therians, and Marsupials* (ed. F. S. Szalay, M. J. Novacek and M. C. McKenna), pp. 165-181. New York, NY: Springer-Verlag.
Moore, W. J. (1981). *The Mammalian Skull*. Cambridge, UK: Cambridge University Press.
Mozell, M. M., Sheehe, P. R., Swieck, S. W., Jr, Kurtz, D. B. and Hornung, D. E. (1984). A parametric study of the stimulation variables affecting the magnitude of the olfactory nerve response. *J. Gen. Physiol.* **83**, 233-267.
Oka, Y., Takai, Y. and Touhara, K. (2009). Nasal airflow rate affects the sensitivity and pattern of glomerular odorant responses in the mouse olfactory bulb. *J. Neurosci.* **29**, 12070-12078.
Smith, T. D. and Rossie, J. B. (2008). Nasal fossa of mouse and dwarf lemurs (primates, Cheirogaleidae). *Anat. Rec.* **291**, 895-915.
Smith, T. D., Eiting, T. P. and Rossie, J. B. (2011). Distribution of olfactory and nonolfactory surface area in the nasal fossa of *Microcebus murinus*: implications for microcomputed tomography and airflow studies. *Anat. Rec.* **294**, 1217-1225.
Smith, T. D., Eiting, T. P. and Bhatnagar, K. P. (2012). A quantitative study of olfactory, non-olfactory, and vomeronasal epithelia in the nasal fossa of the bat *Megaderma lyra*. *J. Mamm. Evol.* **19**, 27-41.
Smith, T., Eiting, T. and Bhatnagar, K. (in press). Anatomy of the nasal passages in mammals. In *Handbook of Olfaction and Gustation*, 3rd edn (ed. R. Doty). New York, NY: Wiley.
Thies, W., Kalko, E. K. V. and Schnitzler, H. U. (1998). The roles of echolocation and olfaction in two Neotropical fruit-eating bats, *Carollia perspicillata* and *C. castanea*, feeding on *Piper*. *Behav. Ecol. Sociobiol.* **42**, 397-409.
Tucker, D. (1963). Physical variables in the olfactory stimulation process. *J. Gen. Physiol.* **46**, 453-489.
Van Valkenburgh, B., Theodor, H., Friscia, A., Pollack, A. and Rowe, T. (2004). Respiratory turbinates of canids and felids: a quantitative comparison. *J. Zool.* **264**, 281-293.
Yang, G. C., Scherer, P. W. and Mozell, M. M. (2007). Modeling inspiratory and expiratory steady-state velocity fields in the Sprague-Dawley rat nasal cavity. *Chem. Senses* **32**, 215-223.
Zhao, K., Dalton, P., Yang, G. C. and Scherer, P. W. (2006). Numerical modeling of turbulent and laminar airflow and odorant transport during sniffing in the human and rat nose. *Chem. Senses* **31**, 107-118.